Research Square

Preprints are preliminary reports that have not undergone peer review.
They should not be considered conclusive, used to inform clinical practice,
or referenced by the media as validated information.

Targeted Dual-Modality Imaging of Pisum Sativum Agglutinin Functionalized $CuFeSe_2$ Nanoparticles for Enhanced Cholangiocarcinoma Diagnosis

Jing Zhang
The Affiliated Hospital of Southwest Medical University
Yaolin Gong
The Affiliated Hospital of Southwest Medical University
Wenlu Li
The Affiliated Hospital of Southwest Medical University
Yuda Zhu
The Affiliated Hospital of Southwest Medical University
Wen Xiu Ren
The Affiliated Hospital of Southwest Medical University
Jian Shu
shujiannc@163.com

The Affiliated Hospital of Southwest Medical University https://orcid.org/0000-0002-7386-7217

Research Article

Keywords: Cholangiocarcinoma (CCA), Dual-Modality Imaging, CuFeSe2 Nanoparticles, Pisum Sativum Agglutinin (PSA), Magnetic resonance imaging (MRI), Computed Tomography (CT)

Posted Date: September 30th, 2025

DOI: https://doi.org/10.21203/rs.3.rs-7591535/v1

License: This work is licensed under a Creative Commons Attribution 4.0 International License.
Read Full License

Abstract

Purpose: To improve cholangiocarcinoma (CCA) diagnosis by exploiting pisum sativum agglutinin (PSA) to target mannose-type N-glycans over-expressed on CCA cells, and to evaluate $CuFeSe_2$-PSA nanoparticles as a dual-modality contrast agent for T2-weighted MRI and CT imaging.

Procedures: $CuFeSe_2$ nanoparticles were surface-functionalized with PSA. Their physicochemical properties, dispersity, biosafety, and dual-contrast capability (T2-MRI and CT) were assessed in vitro. Targeting specificity toward CCA cells and tissues was examined with both in vitro cellular assays and in vivo animal models.

Results: Functionalization with PSA improved nanoparticle dispersity and biosafety. The resulting $CuFeSe_2$-PSA nanoparticles provided effective contrast enhancement for both T2-MRI and CT. In vitro and in vivo experiments showed that PSA markedly increased the probe's recognition and accumulation in CCA cells and tumor tissues, leading to prominently enhanced tumor contrast and delineation.

Conclusions: $CuFeSe_2$-PSA nanoparticles constitute a novel diagnostic platform that enables precise dual-modality imaging of CCA and hold potential for future therapeutic applications, offering a promising approach for clinical CCA diagnosis.

1. Introduction

Cholangiocarcinomas (CCAs) are a highly aggressive malignant carcinoma originating from the bile duct epithelial cells. Based on their anatomical location, CCAs are clinically characterized as intrahepatic, extrahepatic, or hilar cancers[1]. Although the global incidence of CCAs is low, accounting for only 3% of all malignant tumor diseases, the prognosis of CCAs is extremely poor due to its highly aggressive and difficult-to-diagnose at early stage[2, 3]. The 5-year survival rate is less than 10%[4]. The main reason for such a high mortality rate is the delay in diagnosis and lack of effective treatment for late-stage CCAs[4]. The etiology of CCAs is complex and unclear, some recognized high-risk factors include cirrhosis, bile duct stones, liver fluke infection, persistent bile duct inflammation (such as primary sclerosing cholangitis), and specific genetic abnormalities[5]. Most patients with CCA occurring have no symptoms, which is also an important reason for its difficult-to-diagnose at early stage[3, 5]. Some early clinical symptoms of CCAs patients are frequently nonspecific, such as moderate jaundice, abdominal pain, and weight loss, which may lead to misdiagnosis as other hepatobiliary system disorders[2]. Clinically, serologic marker tests, tissue biopsies, and imaging modalities are commonly employed in the diagnosis of CCAs[4]. However, these methods are faced with the disadvantages of low sensitivity, difficult sample acquisition and poor specificity. For instance, due to the lack of accurate specificity, the increased serum markers glycoconjugation antigen 19 – 9 (CA19-9) and carcinoembryonic antigen (CEA) in CCAS patients are also misdiagnosed as other hepatobiliary diseases[5, 6].

Currently, medical imaging examination is an essential means of clinical diagnosis of CCAs, including positron emission tomography (PET), magnetic resonance imaging (MRI), computed tomography (CT)

and ultrasonography (US). However, for the early stages of CCAs, traditional imaging detection has low sensitivity and specificity, failuring in accurately identify minimal lesions or tumor tissue boundaries[7, 8]. Therefore, how to improve the sensitivity and specificity of CCAs imaging results has exert a peculiar fascination on a great many researchers. In contemporary oncology, molecular imaging is a fast-growing discipline which using probes to target tumor-specific markers for clearly identify malignant tissues from normal tissues on imaging[9]. The advances in nanotechnology have made it easier to construct and optimize molecular imaging probes for tumor-specific imaging, not only for early diagnosis of tumors, but also for subsequent treatment with an integrated theranostic platform[10, 11]. Modifying nanoprobes with targeted molecules that can recognize signature markers on tumor cells surface or in their microenvironment is expected to enhance their targeted enrichment and imaging signals at the tumor site[10, 12]. In addition, the versatility of the nanoprobes could enable the fusion of multiple diagnostic imaging modalities to obtain high-contrast soft tissue imaging and high-resolution anatomical structure imaging at once, overcoming the shortcomings of a single imaging result[13, 14]. These designs show particularly important for early diagnosis of CCAs, rapid diagnosis of lesion location and accurate differentiation of tumor and surrounding tissue.

In order to improve the accuracy of CCAs diagnosis, the key is to apply targeted molecules that could specifically identify markers characteristic of CCA tumors. It has been widely acknowledged that aberrant N-glycan chain structures are highly expressed in CCA cells, particularly in those with high aggression[15, 16]. These N-glycosyl chains play a role in not only the proliferation, migration, and invasiveness of cancer cells but also the development of the tumor microenvironment[17–19]. Therefore, these N-glycosyl chains allow for the targeted enrichment of contrast agents at CCAs tumor sites, thereby improving the accuracy and clarity of clinical imaging[20]. Pisum sativum agglutinin (PSA), a protein generated from plants called pea agglutinin, can bind to specific sugar groups and is widely used to label sugar molecules on the surface of cells[20, 21]. Thus, it could be of great significance to investigate whether PSA could improve the CCAs cell recognition by contrast agents and enhance the imaging effect of tumor tissue.

In this work, $CuFeSe_2$ contrast agents with uniform nano-morphology and well monodispersity were fisrt fabricated by a solvothermal method. As a ternary chalcogenide semiconductor materials, $CuFeSe_2$ exhibit excellent magnetic, electrical and optical properties. Due to the presence of both Cu and Fe, $CuFeSe_2$ can act as a multimodality imaging contrast agent for both MRI and CT. Compared with the widely used gadobutrol or iodinated contrast agents in clinical, $CuFeSe_2$ propose better water solubility, colloid stability, Biocompatibility and versatility. We then modified PSA on the surface of the $CuFeSe_2$ agents to enhance their affinity for N-glycosyl chains on CCAs cells surfaces. In vitro and in vivo experiments demonstrated that PSA modification could enhance the uptake efficiency of the $CuFeSe_2$ agents by CCAs cells, and enhance the MRI and CT imaging signal of tumor tissues. Sum up, $CuFeSe_2$-PSA agents exhibit tremendous promise in the imaging diagnosis of CCAs, offering a fresh approach to enhancing both therapeutic efficacy and diagnostic precision.

2. Materials and Methods

2.1. Materials

Selenium powder (Se, ≥ 99.5%), sodium borohydride ($NaBH_4$, ≥ 99%), copper(II) chloride dihydrate ($CuCl_2·2H_2O$), ferrous sulfate heptahydrate ($FeSO_4·7H_2O$), RPMI-1640 medium, and fetal bovine serum (FBS) were obtained from Sigma-Aldrich (USA). $SM(PEG)_{24}$, a PEGylated long-chain SMCC crosslinker, and NeutrAvidin Protein (Neu) were purchased from Thermo Scientific (USA). 2-Iminothiolane hydrochloride (Traut) was purchased from Aladdin Reagent (China), and Pisum Sativum Agglutinin (PSA) was obtained from Vector Laboratories (UK). Dialysis bags with molecular weight cutoffs of 3K and 100K were acquired from Shanghai Yuanye Biotechnology (China). PBS (pH 7.2–7.4) was purchased from Solarbio (China). All chemicals were used as received without further purification.

2.2. Methods

2.2.1. Synthesis of $CuFeSe_2$ and $CuFeSe_2$-NH_2

The synthesis of $CuFeSe_2$ was carried out following a previously described method[22]. To begin, 80 mg of selenium powder and 82 mg of $NaBH_4$ were dispersed in 50 mL of deionized water within a two-neck flask. The mixture was stirred under nitrogen protection for 1 hour, during which the solution gradually changed color from dark gray to colorless. Next, 140 mg of $FeSO_4·7H_2O$ and 86 mg of $CuCl_2·2H_2O$ were dissolved in 5 mL of deionized water and immediately added to the flask. The reaction mixture was stirred at room temperature for 2 hours, resulting in the solution turning black, indicating the successful synthesis of $CuFeSe_2$ nanoparticles. After the reaction was complete, 200 µL of (3-Aminopropyl) triethoxysilane (APTES) was added to the mixture, which was then stirred continuously for an additional 12 hours. The resulting product was washed thoroughly with deionized water and subjected to centrifugation at 9000 rpm for 15 minutes. This washing and centrifugation process was repeated three times to obtain the final product, $CuFeSe_2$-NH_2.

2.2.2. Synthesis of $CuFeSe_2$-Neu and $CuFeSe_2$-PSA

To obtain the $CuFeSe_2$-Neu nanoparticles, 50 mg of the powder was dissolved in 25 mL of PBS at room temperature, followed by the addition of 35.5 µL of $SM(PEG)_{24}$ crosslinker solution (250 mmol/L in DMSO). After 30 minutes of magnetic stirring in a dark environment, the solution was dialyzed against PBS using a 3K dialysis membrane for 24 hours, yielding $CuFeSe_2$-SMPEG nanoparticles. The $CuFeSe_2$-Neu nanoparticle solution was obtained by dialyzing in pure water using a 100K dialysis bag for 24 hours after 2.3 mL of NeutrAvidin Protein (Neu) solution (1 mg/mL, purified water) and 2.3 mL of PBS solution were combined. 100 uL of 2-iminothiocyclopentane hydrochloride (Traut) reagent (1 mg/mL, purified water) was then added and the mixture was thoroughly mixed. The solution was then incubated for one hour in the dark. To further conjugate PSA, 10 mg of biotinylated PSA was added to the $CuFeSe_2$-Neu

solution, followed by incubation and subsequent dialysis using a 100K membrane for 24 hours, resulting in $CuFeSe_2$-PSA nanoparticles.

2.2.3. Characterization

Transmission electron microscopy (TEM) was utilized to capture high-resolution images and investigate the morphological features of $CuFeSe_2$-NH_2, $CuFeSe_2$-Neu, and $CuFeSe_2$-PSA. The particle size distribution of these samples was accurately measured using Nano Measure software, providing detailed quantitative insights. To further analyze their structural properties, cobalt target wide-angle X-ray diffraction (XRD) was performed on $CuFeSe_2$-NH_2 and $CuFeSe_2$-PSA with the help of an X-ray powder diffractometer. This method enabled precise characterization of their crystalline phases and structural arrangements. The elemental composition and concentrations of key elements, including Cu, Fe, and Se, in $CuFeSe_2$-PSA were quantified using inductively coupled plasma optical emission spectroscopy (ICP-OES), ensuring reliable and accurate measurements. Additionally, Fourier transform infrared spectroscopy (FTIR) was conducted to validate the chemical structures and confirm the successful synthesis of $CuFeSe_2$-NH_2, $CuFeSe_2$-Neu, and $CuFeSe_2$-PSA.

2.2.4. Cytotoxicity Assays

To evaluate the cytotoxicity of $CuFeSe_2$-PSA on HUCCT1 and HIBEC cells, a cell counting kit-8 (CCK-8) assay was performed. Both cell types were maintained in RPMI-1640 complete medium at 37°C with 5% CO_2. Cells were seeded into 96-well plates at a density of 1×10^6 cells per well and incubated for 24 hours. After this, varying concentrations of $CuFeSe_2$-PSA (10, 20, 40, 60, 80, 100, and 150 μg/mL) were added, and the cells were incubated for an additional 24 hours. The CCK-8 assay was then used to determine the cell survival rate.

2.2.5. In Vitro Targeting Evaluation

To evaluate the targeting efficiency of $CuFeSe_2$-PSA nanoparticles, HUCCT1 and HIBEC cells were plated in confocal culture dishes at a concentration of 1×10^4 cells/mL and cultured for 24 hours. Following this, the cells were exposed to $CuFeSe_2$-PSA nanoparticles for a duration of 4 hours. Subsequently, the cells were rinsed three times with PBS to remove unbound particles, and optical microscopy was employed to visualize and analyze the nanoparticle binding.

2.2.6. MR and CT Performance In vitro and In vivo

T2-weighted magnetic resonance imaging (MRI) was performed using a Siemens Prisma 3.0T scanner to analyze the T2 signal intensities of solutions with varying concentrations. The imaging parameters included an echo time (TE) of 70 ms, repetition time (TR) of 3000 ms, field of view (FOV) dimensions of 30×60×25 mm, slice thickness of 1.0 mm, slice spacing of 0.15 mm, a matrix resolution of 256×256, and an area of interest measuring 20 mm^2. For in vivo imaging involving animal models, tumor cross-sections were identified following the scans, and specific regions of interest (ROIs) were defined for each tumor. The variations in T2 values were examined within a region of 5 mm^2.

CT imaging was conducted using a Philips IQon CT scanner to measure the CT values of the concentrated solutions. The CT parameters were as follows: a tube voltage of 120 kV, tube current of 100 mAs, energy level of 40 keV, FOV of 150 mm, matrix resolution of 512×512, slice thickness of 0.14 mm, window width of 200, and window level of 80. In the animal model experiments, tumor ROIs were delineated post-scan, and CT values within the tumors were recorded. The window width and level were subsequently adjusted to 350 mm and 60 mm, respectively, with measurements confined to an area of 5 mm^2.

2.2.7. Tumor Model

All animal experiments were conducted in strict accordance with the protocols approved by the Laboratory Animal Welfare and Ethics Committee of Southwest Medical University (Approval No. 20210811–25). These protocols were designed to ensure full compliance with the *Laboratory Animal Welfare and Ethical Review Guidelines* (GB/T35892–2018), which were established as part of the National Standards of the People's Republic of China. The study also adhered to the ethical principles outlined in the *National Institutes of Health Guide for the Care and Use of Laboratory Animals* (NIH Publications No. 8023, revised 1978), ensuring the humane treatment and care of all animals used in the research.

For the study, female BALB/c nude mice, aged 6–8 weeks and weighing 15–22 g, were purchased from Sipeifu (Beijing). These immunodeficient mice were selected due to their suitability for xenograft tumor models, as they lack the ability to mount a full immune response, which facilitates tumor growth and experimental observation. The mice were housed in pathogen-free conditions, with controlled temperature, humidity, and a 12-hour light-dark cycle, and were provided with food and water ad libitum to ensure optimal health and well-being during the experiment.

To establish tumor-bearing models, HUCCT1 cells (2×10^6 per mouse) were subcutaneously injected into the dorsal region of each mouse. The site of injection was carefully prepared under sterile conditions to prevent contamination, and the mice were monitored closely during the post-injection period for signs of discomfort or distress. Tumor formation was confirmed when the tumor volume reached approximately 100 mm^3, as calculated using the formula Volume = (length × width × width) /2. At this stage, the models were considered successfully established and suitable for subsequent experimental procedures.

3. Results

3.1. Nanoparticle Characterization

Nanoparticles are widely used in biomedicine on account of their easy surface modification. By introducing targeting molecules PSA, nano-contrast agents are expected to be enriched at the tumor site of CCAs. In the present study, we first synthesized $CuFeSe_2$ nanoparticles using an aqueous phase synthesis method and introduced amino groups on their surface by modifying APTES, followed by

grafting the bridging molecule SM(PEG)$_{24}$ on their surfaces via an amidation reaction. Secondly, the thioether bond formed by the interaction between maleimide and with thiol group was used to modify the thiolated-avidin onto the nanoparticles. Finally, utilizing the affinity of avidin with biotin, PSA was successfully attached to the $CuFeSe_2$ nanoparticles. Transmission electron microscopy (TEM) and Dynamic light scattering (DLS) were used to detect the change of nanoparticles morphology and size during the reactions (Fig. 1a-c, Figure S1). As revealed by TEM pictures, $CuFeSe_2$-NH_2 has lamellar structures with a nanoparticle size of about 125 nm. With the gradual grafting of Neu and PSA groups, the size of nanoparticles gradually increased, while $CuFeSe_2$-Neu and $CuFeSe_2$-PSA have average diameters of 260 and 310 nm, respectively. Similar results can also be obtained from the DLS test, with a gradual increase in particle size from the initial 140 nm to the final nearly 390 nm as the reactions proceed. These results demonstrate the successful modification of PSA on $CuFeSe_2$ nanoparticles.

The chemical composition of $CuFeSe_2$-PSA was further verified by energy-dispersive X-Ray spectroscopy (EDX) analysis (Fig. 1d). The elements of copper, iron, selenium, and nitrogen were evenly distributed throughout the nanoparticles, suggesting that multi-step functional modifications had little impact on the overall structure of the $CuFeSe_2$. The molar ratio of Cu, Fe and Se were found to be highly consistent with the intended 1:1:2 stoichiometric ratio, as demonstrated by Inductively coupled plasma atomic emission spectroscopy (ICP-AES) measurements (Figure S2). These results further confirmed the accuracy of the nanoparticle compositions and the dependability of the synthesis method. According to X-ray diffraction (XRD) analysis (Fig. 1e), both $CuFeSe_2$-NH_2 and $CuFeSe_2$-PSA nanoparticles contain strong reflection peaks, which are compatible with the tetragonal prismatic structure (JCPDS No. 81-1959). Notably, there was a modest shift in the XRD diffraction peaks of $CuFeSe_2$-PSA, which may be attributed to slightly altered nanoparticles lattice characteristics by the influence of PSA molecules. Fourier transform infrared spectroscopy (FTIR) images clearly showed the characteristic peaks of C-N and C = O stretching vibrations, confirming the presence of PSA on $CuFeSe_2$ nanoparticle surfaces (Fig. 1f).

The $CuFeSe_2$ nanoparticle has proven to possess a relatively high X-ray attenuation coefficient for CT imaging. The CT imaging ability of $CuFeSe_2$-PSA displayed a concentration dependent brightening effect at 80 kV (Fig. 2a). In addition, the Hounsfield units (HU) value linearly increased with the increase in nanoparticle centration, suggesting a remarkable CT contrast ability (Fig. 2b). $CuFeSe_2$-PSA enjoys the ability of MR imaging due to the existence of the paramagnetic metal element of Fe. The T_1 relaxivity (r_1) of $CuFeSe_2$-PSA was measured to be 0.99 $mM^{-1}s^{-1}$ under 3.0 T (Fig. 3a, 3c). Besides, the T_2 relaxivity (r_2) of $CuFeSe_2$-PSA was calculated to 156.32 $mM^{-1}s^{-1}$ and the ultra-high r_2/r_1 ratio (158.97) of $CuFeSe_2$-PSA render it a remarkable T_2-weighted MR imaging contrast agent (Fig. 3b, 3d). In addition, the T_2-weighted MR images of $CuFeSe_2$-PSA showed an obvious concentration-dependent brightening effect. These above results demonstrate that $CuFeSe_2$-PSA has potential application in dual-modality CT and MRI imaging.

3.2. In vitro cytotoxicity and targeting

Before verifying the in vivo imaging effect of $CuFeSe_2$-PSA, we first examined the biological safety of nanoparticles, which is one of the essential properties for biomedical materials. In this investigation, cytotoxicity experiments were carried out on both the cholangiocarcinoma cell line, HUCCT1, and the normal biliary epithelial cell line, HIBEC. After the cells were incubated with different concentrations of $CuFeSe_2$-PSA nanoparticles (10–150 μg/mL) for 24 hours, the viability of the cells was detected by a CCK-8 detection kit. As shown in Fig. 4a, both HIBEC cells and HUCCT1 cells showed high cell viability, with a survival rate kept over 90% even at the highest $CuFeSe_2$-PSA concentration. Such low cytotoxicity of the material can be attributed to the following factors: (1) the high chemical structure stability reduces the amount of toxic metal ions that may be released into the cell environment, thus reducing the cytotoxicity of $CuFeSe_2$-PSA, (2) the modification of PSA protein structure further improves the biological safety of $CuFeSe_2$-PSA nanoparticles. It has been proven that PSA can specifically bind to the N-glycosyl chains on cancer cells surfaces, thus enhancing the uptake of the nanoparticles by tumor cells. Using confocal microscopy, we compared the distribution of the nanoparticles in the cholangiocarcinoma cell line HUCCT1 and the normal epithelial cell line HIBEC to demonstrate the targeting of $CuFeSe_2$-PSA (Fig. 4b). After the cells and $CuFeSe_2$-PSA were incubated for 4 h, an obvious accumulation of nanoparticles could be observed in the cytoplasm of HUCCT1 cells. In contrast, no discernible accumulation was observed in normal cells. The results showed that PSA could effectively enhance the specific enrichment ability of $CuFeSe_2$ to HUCCT1 cells, which lines the prerequisite for in vivo targeted imaging.

3.3. In vivo biosafety

Furthermore, the $CuFeSe_2$-PSA nanoparticles were administered intravenously into a healthy nude mouse model, and the mice were monitored continuously for 15 days to assess the biosafety of the nanoparticles. During the 15-day observation period, neither behavioral abnormalities nor weight loss was observed in mice, indicating good tolerance of $CuFeSe_2$-PSA. Moreover, on the last day of the observation period, the mice were euthanized and their major organs (heart, liver, spleen, lung and kidney) were extracted for hematoxylin and eosin (H&E) staining (Fig. 5). There was no evident histological abnormalities, inflammatory reactions, or tissue damage were found in the tissue sections of the major organs, providing additional evidence for the biosafety of $CuFeSe_2$-PSA.

3.4. In vivo dual-modality imaging

We further constructed the CCAs mouse tumor model to validate the in vivo MRI and CT dual-modality imaging effect of $CuFeSe_2$-PSA. The experimental results showed that the intravenous injection of $CuFeSe_2$-PSA could significantly improve the MRI and CT signals at the tumor site. Specifically, for the $CuFeSe_2$-PSA treated group, the T_2-weighted signal intensity in the tumor area decreased significantly at

4 h after intravenous injection, which was due to the enrichment of $CuFeSe_2$-PSA at the tumor site (Fig. 6a). In contrast, the non-targeted $CuFeSe_2$-Neu exhibited moderate T_2-weighted signal alterations, which was dependent on the non-specific accumulation of nanoparticles through the EPR effect. The concentration of $CuFeSe_2$-PSA at the tumor site was further verified by CT imaging (Fig. 6b). Following injection, there was a considerable rise in the CT values at the tumor location for the $CuFeSe_2$-PSA treated group, which was similar with MRI results. According to a quantitative study, $CuFeSe_2$-PSA nanoparticles significantly outperformed the non-targeted group in terms of increasing tumor MRI and CT contrast (Figure S3). Considering that MRI with high soft-tissue resolution can distinguish well between the tumor and surrounding tissues, while CT imaging displays more anatomical structural details. $CuFeSe_2$-PSA with dual-modality imaging capability may give a more thorough tumor image and assist medical professionals in making more precise assessments of the size, location, and appearance of CCAs tumors.

4. Discussion and conclusion

The insidious incidence of CCAs and difficult early diagnosis has long been puzzling clinicians[23]. Medical imaging modalities based on MRI and CT are widely utilized diagnostic methods for CCAs in clinical settings. However, due to the intricate tumor microenvironment of CCAs, their ability to accurately detect early lesions and identify tumor invasion boundaries remains limited[24, 25]. It is urgent to develop novel imaging probe with high CCAs tumour targeting and high resolution. In this study, taking advantage of the specific binding properties of PSA to N-glycosyl chains on cancer cells, we constructed a dual-mode imaging probe $CuFeSe_2$-PSA with in vivo CCAs targeting ability for high-contrast MRI and CT diagnosis. Our work provides new opportunities for enhancing the early detection of CCAs while line the groundwork for future focused diagnostic and treatment approaches.

It is worth noting that the overexpression of N-glycosyl chains on CCA cells surfaces is one of remarkable physiological characteristics, which is closely related to their invasiveness and metastasis[26, 27]. Pisum sativum agglutinin (PSA) is a molecule that recognizes N-glycosyl chains preferentially, and its modification on the surface of nano-probe can effectively improve their efficiency of targeted enrichment to CCA cells in vivo[20]. Such a combination of nanotechnology and medical image detection can accurately localize tumor tissue, which is beneficial for tumor early diagnosis and evaluation of their invasion and metastasis. The experimental results also showed a considerable improvement of in vivo CCAs tumor tissue MRI and CT imaging for $CuFeSe_2$-PSA nanoparticles. Compared to traditional CT and MRI scans, $CuFeSe_2$-PSA could greatly increase the sensitivity and specificity of imaging, enabling the early diagnosis of malignancies. Moreover, the dual-mode imaging capability of $CuFeSe_2$-PSA provides a more comprehensive diagnostic tool for clinical detection, offering a comprehensive assessment including tumor location, size, morphology and its association with surrounding tissues. It has been known that MRI can offer high-contrast soft tissue imaging, while CT performs excellent at displaying anatomical features. This information is essential to determine surgical resection parameters and to track postoperative recurrence.

Our research also needs further exploration. Although we have demonstrated that PSA modification can achieve a precisely targeted recognition of $CuFeSe_2$ nanoparticles to N-glycosyl chains on CCAs cells surfaces. Considering the heterogeneity of tumor cells from different patients and varied N-glycosyl chains expression for different CCAs subtypes. It will be necessary for subsequent studies to examine the effectiveness of PSA to other CCAs subtypes and to combine with other potential targeting molecules (integrins or EGF) for higher accuracy. Secondly, in this study, we only preliminarily verified the low cytotoxicity and short-term biosafety of $CuFeSe_2$-PSA. To guarantee the therapeutic applications of $CuFeSe_2$-PSA in clinical, future research should concentrate on assessing the metabolic pathways, immunological responses, and long-term toxicity of in vivo.

In conclusion, we have fabricated a unique $CuFeSe_2$-PSA contrast agent in this work and showed its potential application in diagnosing CCAs. Taking advantage of the specific recognition of n-glycan chains on cells surfaces by PSA molecules, the $CuFeSe_2$-PSA could specifically enrich at tumor location in vivo and significantly improve the MRI and CT imaging signal of tumor tissues. $CuFeSe_2$-PSA nanoparticles present novel opportunities for enhancing CCA early diagnosis and offering fresh approaches to customized care and diagnostic fusion.

Declarations

Author Contributions

Jing Zhang: conceptualization, data curation, formal analysis, investigation, writing – original draft. Yaolin Gong: data curation, formal analysis, investigation, validation. Wenlu Li: data curation, formal analysis, investigation. Yuda Zhu: funding acquisition, visualization, writing – review & editing. Wen Xiu Ren: methodology, project administration, supervision, writing – review & editing. Jian Shu: funding acquisition, resources, supervision, writing – review & editing.

Conflicts of interest

There are no conflicts to declare.

Acknowledgments

This work was supported by National Natural Science Foundation of China, 82272077, the Sichuan Provincial Natural Science Foundation Project, 2024NSFSC0713. This work also was technically supported by the Public Platform of Advanced Detecting Instruments, Public Center of Experimental Technology, Southwest Medical University.

References

1. Yang T, Deng Z, Xu L, Li X, Yang T, Qian Y, Lu Y, Tian L, Yao W, Wang J (2022) Macrophages-aPKC-CCL5 Feedback Loop Modulates the Progression and Chemoresistance in Cholangiocarcinoma. J

Exp Clin Cancer Res 41:23. https://doi.org/10.1186/s13046-021-02235-8

2. Bridgewater J, Galle PR, Khan SA, Llovet JM, Park J-W, Patel T, Pawlik TM, Gores GJ (2014) Guidelines for the diagnosis and management of intrahepatic cholangiocarcinoma. J Hepatol 60:1268–1289. https://doi.org/10.1016/j.jhep.2014.01.021
3. Brindley PJ, Bachini M, Ilyas SI, Khan SA, Loukas A, Sirica AE, Teh BT, Wongkham S, Gores GJ (2021) Cholangiocarcinoma, Nat Rev Dis Primers 7 65. https://doi.org/10.1038/s41572-021-00300-2
4. Banales JM, Cardinale V, Carpino G, Marzioni M, Andersen JB, Invernizzi P, Lind GE, Folseraas T, Forbes SJ, Fouassier L, Geier A, Calvisi DF, Mertens JC, Trauner M, Benedetti A, Maroni L, Vaquero J, Macias RIR, Raggi C, Perugorria MJ, Gaudio E, Boberg KM, Marin JJG, Alvaro D (2016) Expert consensus document: Cholangiocarcinoma: current knowledge and future perspectives consensus statement from the European Network for the Study of Cholangiocarcinoma (ENS-CCA). Nat Rev Gastroenterol Hepatol 13:261–280. https://doi.org/10.1038/nrgastro.2016.51
5. Banales JM, Marin JJG, Lamarca A, Rodrigues PM, Khan SA, Roberts LR, Cardinale V, Carpino G, Andersen JB, Braconi C, Calvisi DF, Perugorria MJ, Fabris L, Boulter L, Macias RIR, Gaudio E, Alvaro D, Gradilone SA, Strazzabosco M, Marzioni M, Coulouarn C, Fouassier L, Raggi C, Invernizzi P, Mertens JC, Moncsek A, Rizvi S, Heimbach J, Koerkamp BG, Bruix J, Forner A, Bridgewater J, Valle JW, Gores GJ (2020) Cholangiocarcinoma 2020: the next horizon in mechanisms and management. Nat Rev Gastroenterol Hepatol 17:557–588. https://doi.org/10.1038/s41575-020-0310-z
6. Lapitz A, Azkargorta M, Milkiewicz P, Olaizola P, Zhuravleva E, Grimsrud MM, Schramm C, Arbelaiz A, O'Rourke CJ, La Casta A, Milkiewicz M, Pastor T, Vesterhus M, Jimenez-Agüero R, Dill MT, Lamarca A, Valle JW, Macias RIR, Izquierdo-Sanchez L, Pérez Castaño Y, Caballero-Camino FJ, Riaño I, Krawczyk M, Ibarra C, Bustamante J, Nova-Camacho LM, Falcon-Perez JM, Elortza F, Perugorria MJ, Andersen JB, Bujanda L, Karlsen TH, Folseraas T, Rodrigues PM, Banales JM (2023) Liquid biopsy-based protein biomarkers for risk prediction, early diagnosis, and prognostication of cholangiocarcinoma. J Hepatol 79:93–108. https://doi.org/10.1016/j.jhep.2023.02.027
7. Fábrega-Foster K, Ghasabeh MA, Pawlik TM, Kamel IR (2017) Multimodality imaging of intrahepatic cholangiocarcinoma. Hepatobiliary Surg Nutr 6:67–78. https://doi.org/10.21037/hbsn.2016.12.10
8. Shin DW, Moon S-H, Kim JH (2023) Diagnosis of Cholangiocarcinoma. Diagnostics (Basel) 13:233. https://doi.org/10.3390/diagnostics13020233
9. Lamarca A, Barriuso J, McNamara MG, Valle JW (2020) Molecular targeted therapies: Ready for prime time in biliary tract cancer. J Hepatol 73:170–185. https://doi.org/10.1016/j.jhep.2020.03.007
10. Liu CH, Grodzinski P (2021) Nanotechnology for Cancer Imaging: Advances, Challenges, and Clinical Opportunities. Radiol Imaging Cancer 3:e200052. https://doi.org/10.1148/rycan.2021200052
11. Lee D-E, Koo H, Sun I-C, Ryu JH, Kim K, Kwon IC (2012) Multifunctional nanoparticles for multimodal imaging and theragnosis. Chem Soc Rev 41:2656–2672. https://doi.org/10.1039/C2CS15261D
12. Radfar R, Akin E, Sehit E, Moldovean-Cioroianu NS, Wolff N, Marquant R, Haupt K, Kienle L, Altintas Z (2024) Synthesis and characterization of core-shell magnetic molecularly imprinted polymer

nanocomposites for the detection of interleukin-6. Anal Bioanal Chem. https://doi.org/10.1007/s00216-024-05536-x

13. Park H, Wang Q (2022) State-of-the-art accounts of hyperpolarized 15N-labeled molecular imaging probes for magnetic resonance spectroscopy and imaging. Chem Sci 13:7378–7391. https://doi.org/10.1039/D2SC01264B
14. Jiang Y, Tian Y, Feng B, Zhao T, Du L, Yu X, Zhao Q (2023) A novel molecular imaging probe [99mTc]Tc-HYNIC-FAPI targeting cancer-associated fibroblasts. Sci Rep 13:3700. https://doi.org/10.1038/s41598-023-30806-6
15. Cavada BS, Pinto-Junior VR, Osterne VJS, Nascimento KS (2018) ConA-Like Lectins: High Similarity Proteins as Models to Study Structure/Biological Activities Relationships. Int J Mol Sci 20:30. https://doi.org/10.3390/ijms20010030
16. Ochoa-Rios S, Blaschke CRK, Wang M, Peterson KD, DelaCourt A, Grauzam SE, Lewin D, Angel P, Roberts LR, Drake R, Mehta AS (2023) Analysis of N-linked Glycan Alterations in Tissue and Serum Reveals Promising Biomarkers for Intrahepatic Cholangiocarcinoma. Cancer Res Commun 3:383–394. https://doi.org/10.1158/2767-9764.CRC-22-0422
17. Kalli M, Stylianopoulos T (2018) Defining the Role of Solid Stress and Matrix Stiffness in Cancer Cell Proliferation and Metastasis. Front Oncol 8. https://doi.org/10.3389/fonc.2018.00055
18. Pinho SS, Reis CA (2015) Glycosylation in cancer: mechanisms and clinical implications. Nat Rev Cancer 15:540–555. https://doi.org/10.1038/nrc3982
19. Phoomak C, Silsirivanit A, Park D, Sawanyawisuth K, Vaeteewoottacharn K, Wongkham C, Lam EW-F, Pairojkul C, Lebrilla CB, Wongkham S (2018) O-GlcNAcylation mediates metastasis of cholangiocarcinoma through FOXO3 and MAN1A1. Oncogene 37:5648–5665. https://doi.org/10.1038/s41388-018-0366-1
20. Silsirivanit A (2021) Glycans: potential therapeutic targets for cholangiocarcinoma and their therapeutic and diagnostic implications. Expert Opin Ther Targets 25:1–4. https://doi.org/10.1080/14728222.2021.1861250
21. Mishra A, Behura A, Mawatwal S, Kumar A, Naik L, Mohanty SS, Manna D, Dokania P, Mishra A, Patra SK, Dhiman R (2019) Structure-function and application of plant lectins in disease biology and immunity. Food Chem Toxicol 134:110827. https://doi.org/10.1016/j.fct.2019.110827
22. Li W, Gong Y, Zhang J, Liu J, Li J, Fu S, Ren WX, Shu J (2024) Construction of CXCR4 receptor-targeted CuFeSe2 nano theranostic platform and its application in MR/CT dual model imaging and photothermal therapy. Int J Nanomed 19:9213–9226. https://doi.org/10.2147/IJN.S470367
23. Sirica AE, Gores GJ, Groopman JD, Selaru FM, Strazzabosco M, Wei Wang X, Zhu AX (2019) Intrahepatic Cholangiocarcinoma: Continuing Challenges and Translational Advances. Hepatology 69:1803–1815. https://doi.org/10.1002/hep.30289
24. Khosla D, Misra S, Chu PL, Guan P, Nada R, Gupta R, Kaewnarin K, Ko TK, Heng HL, Srinivasalu VK, Kapoor R, Singh D, Klanrit P, Sampattavanich S, Tan J, Kongpetch S, Jusakul A, Teh BT, Chan JY,

Hong JH (2024) Cholangiocarcinoma: Recent Advances in Molecular Pathobiology and Therapeutic Approaches, Cancers 16 801. https://doi.org/10.3390/cancers16040801

25. Wang T, Ni Y, Liu L (2024) Innovative Imaging Techniques for Advancing Cancer Diagnosis and Treatment. Cancers 16:2607. https://doi.org/10.3390/cancers16142607
26. Lagarda-Diaz I, Guzman-Partida AM, Vazquez-Moreno L (2017) Legume Lectins: Proteins with Diverse Applications. Int J Mol Sci 18:1242. https://doi.org/10.3390/ijms18061242
27. Hu M, Zhang R, Yang J, Zhao C, Liu W, Huang Y, Lyu H, Xiao S, Guo D, Zhou C, Tang J (2023) The role of N-glycosylation modification in the pathogenesis of liver cancer. Cell Death Dis 14:1–12. https://doi.org/10.1038/s41419-023-05733-z

Schemes

Scheme 1 is available in the Supplementary Files section

Figures

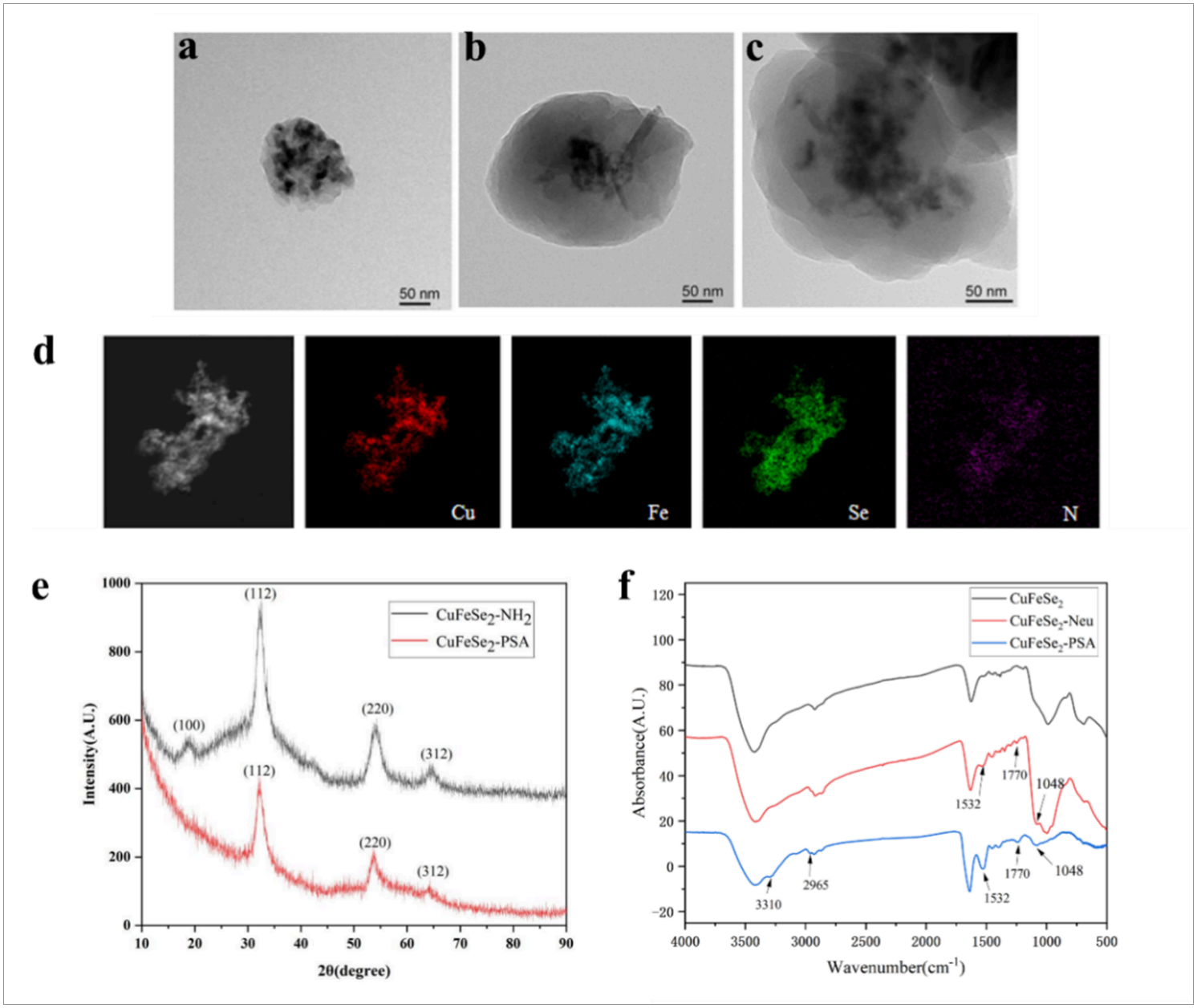


Figure 1

TEM images of (a) $CuFeSe_2$-NH_2, (b) $CuFeSe_2$-Neu and (c) $CuFeSe_2$-PSA nanoparticles; (d) $CuFeSe_2$-PSA with the corresponding elemental mapping of Cu、Fe、Se and N by EDX; (e) X-ray diffraction pattern of $CuFeSe_2$、$CuFeSe_2$-PSA nanoparticles; (f) Fourier infrared spectra of $CuFeSe_2$、$CuFeSe_2$-Neu and $CuFeSe_2$-PSA nanoparticles.

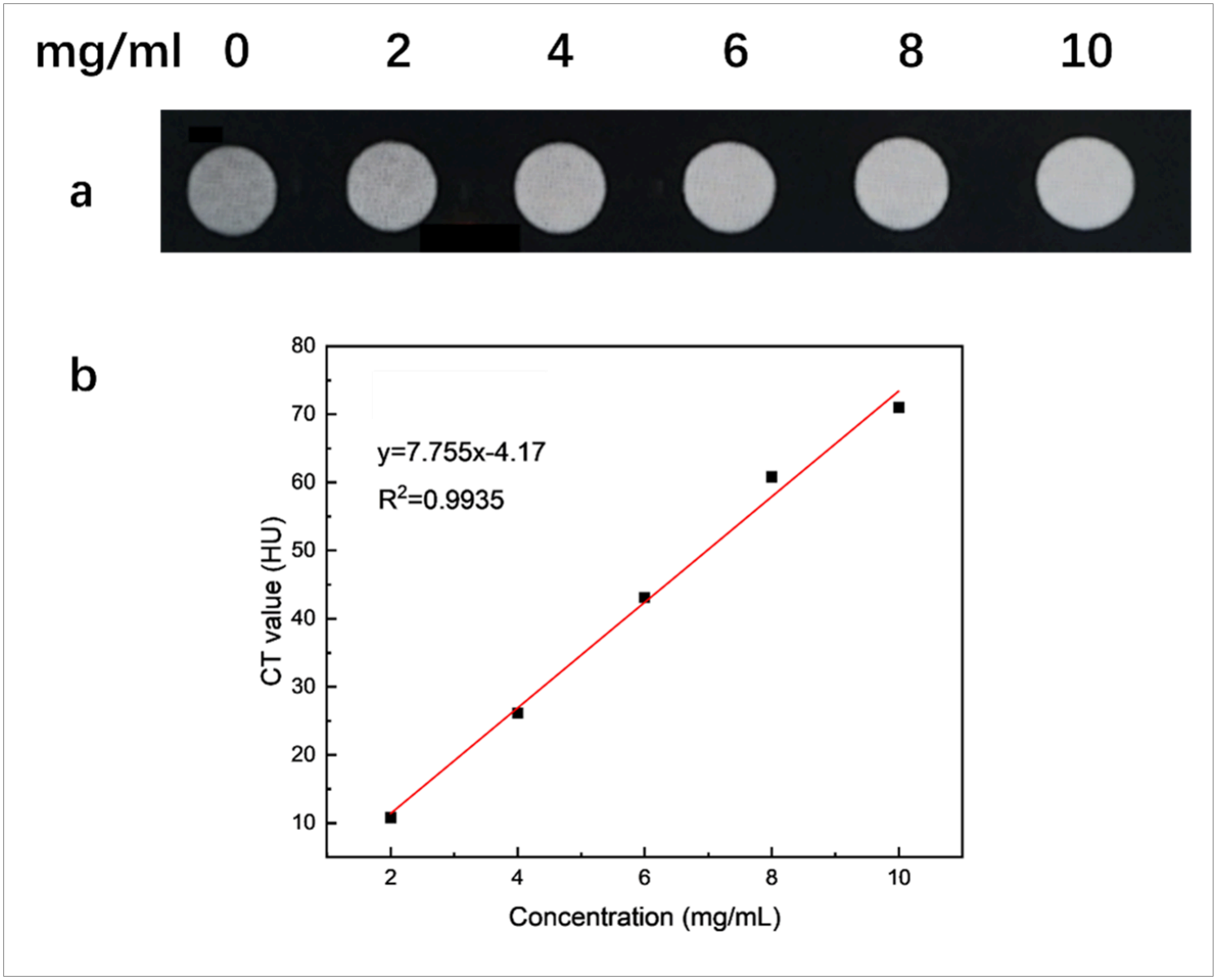


Figure 2

The CT images of $CuFeSe_2$-PSA with different concentrations (a) and the relationship between CT value and concentration (b)

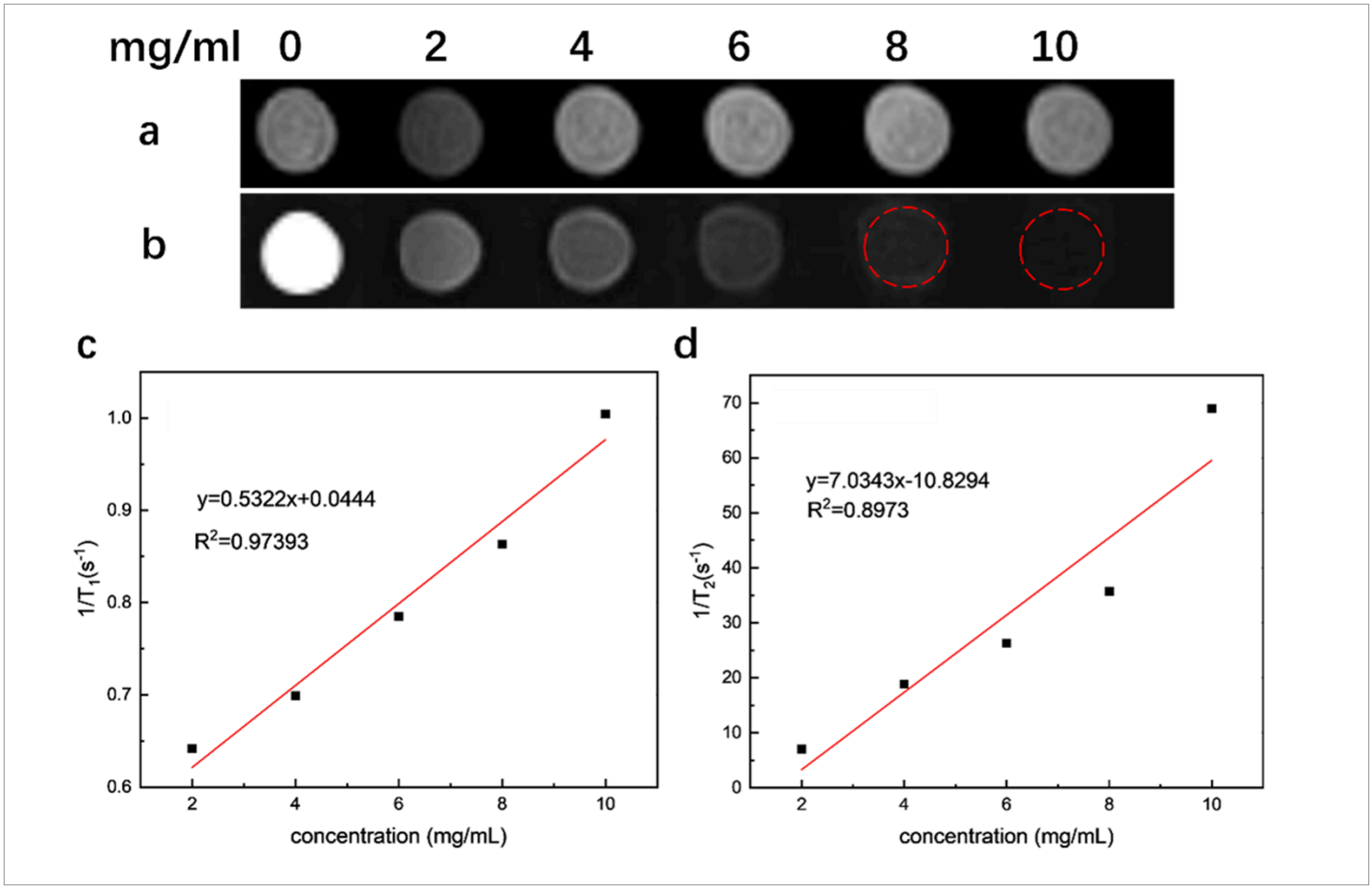


Figure 3

The Magnetic resonance T1 imaging (a) and T2 imaging (b) of CuFeSe2-PSA with different concentrations; Magnetic resonance T1 imaging (c) and T2 imaging (d) of $CuFeSe_2$-PSA with different concentrations.

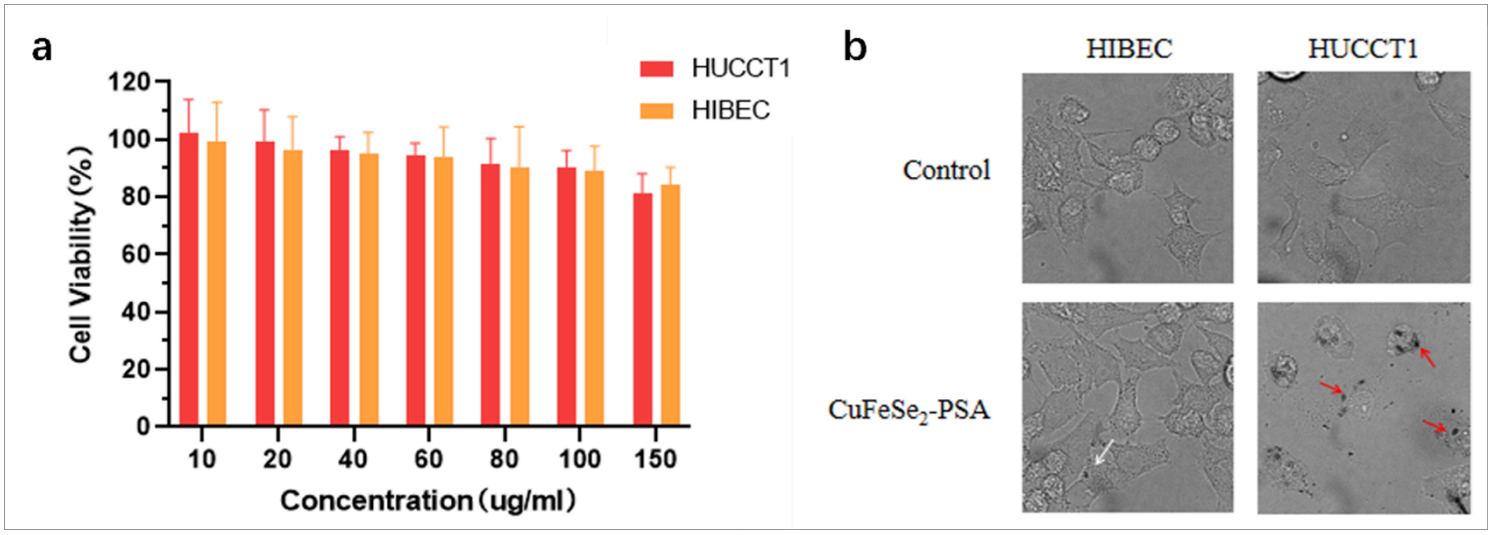


Figure 4

(a) Cell viability of HUCCT1HIBEC cell co-incubated with different concentrations of $CuFeSe_2$-PSA nanoparticles for 24 h; (b) Optical microscope image of 100 ug/ml $CuFeSe_2$-PSA nanoparticles after co-incubation with HUCCT1 and HIBEC cells for 4 hours. The red arrow indicates the $CuFeSe_2$-PSA nanoparticles bound to HUCCT1 cells; the white arrow indicates the $CuFeSe_2$-PSA nanoparticles bound to HIBEC cells.

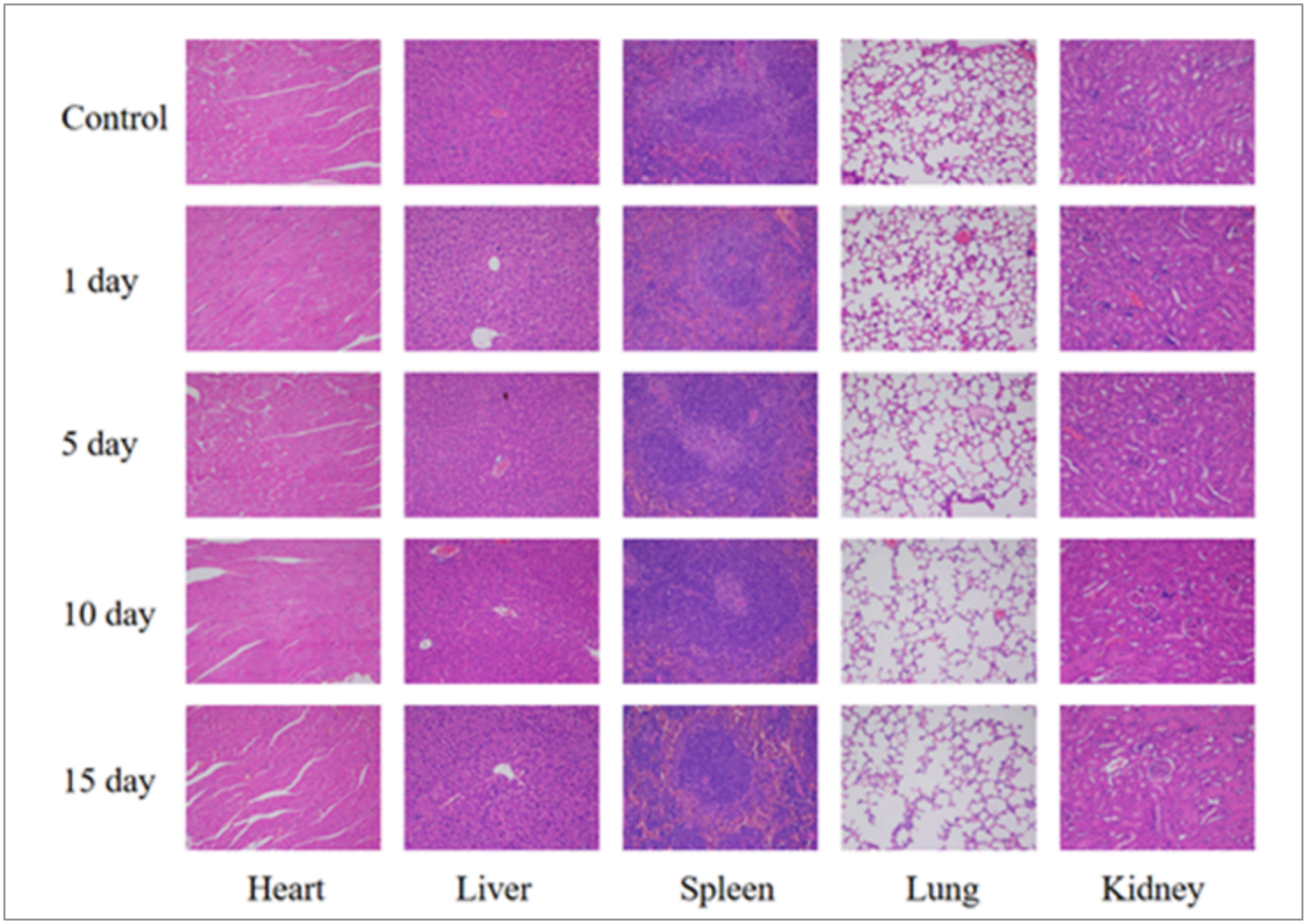


Figure 5

H&E staining of important tissue sections at different time points after injection of $CuFeSe_2$-PSA and PBS into the tail vein of normal mice.

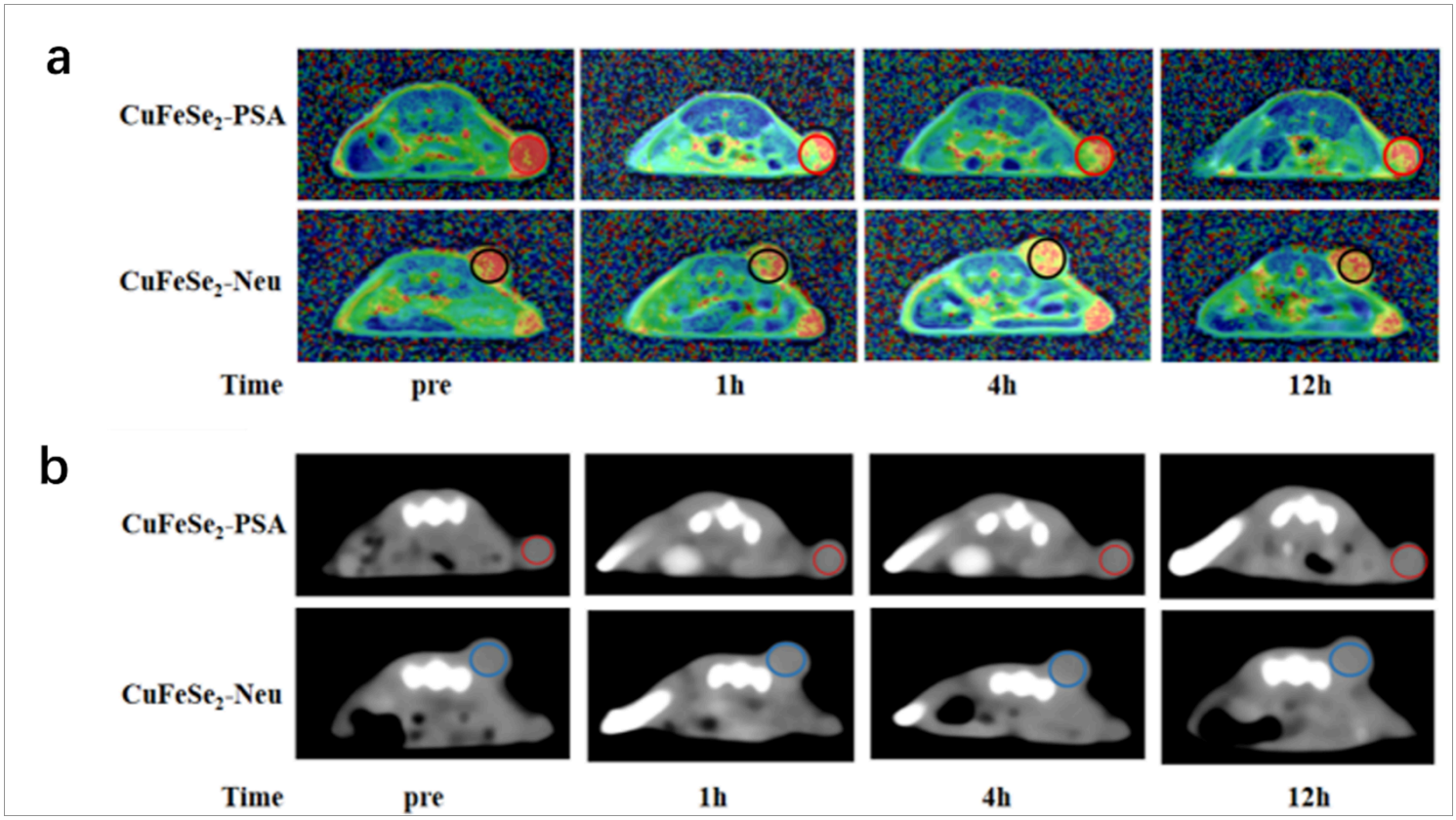


Figure 6

(a) T2 mapping images and (b) CT images of HUCCT1 tumor mice before and after intravenous injection of $CuFeSe_2$-PSA solution.

Supplementary Files

This is a list of supplementary files associated with this preprint. Click to download.

- S1.tif
- S2.tif
- S3.tif
- Scheme1.tif